MAGNETIC RESONANCE IN CHEMISTRY, VOL. 36, 196–204 (1998)

Parameter Estimation for Moisture Transport in Apples with the Aid of NMR Imaging

E. Verstreken,[1] P. Van Hecke,[2] N. Scheerlinck,[1] J. De Baerdemaeker[1] and B. Nicolaï[3]*

[1] Department of Agroengineering and -economics, K.U. Leuven, K. Mercierlaan 92, B-3001 Heverlee, Belgium
[2] Biomedical NMR Unit, Katholieke Universiteit Leuven, O&N Herestraat 49, B-3000 Leuven, Belgium
[3] Flanders Centre for Postharvest Technology, K.U. Leuven, de Croylaan 42, B-3001 Heverlee, Belgium

Received 10 March 1997; Revised 10 September 1997; Accepted 20 September 1997

ABSTRACT: The moisture diffusivity of Jonagold apple flesh and skin was estimated based on NMR images obtained from drying experiments. It was assumed that the diffusivities were not dependent on the moisture concentration. A multi-echo sequence was required to correct for the change of T_2 during the experiment. The diffusivities were estimated by minimization of the squared error between measured and predicted moisture concentrations. The latter were calculated based on the analytical solution or a Galerkin finite element discretization of the diffusion equation. The average flesh diffusivity was 10.3×10^{-11} m^2 s^{-1} and did not change significantly during ultra-low oxygen storage. The corresponding skin diffusivity was 1.32×10^{-13} m^2 s^{-1}. If the flesh and skin diffusivity were estimated simultaneously, the values were 2.8×10^{-12} and 6.3×10^{-15} m^2 s^{-1}, respectively.

KEYWORDS: moisture transport; apples; NMR imaging; parameter estimation

INTRODUCTION

Water transport processes in fruit are important from both the producers' and the consumers' point of view, as they affect the economic benefit and the fruit quality. The economic benefit for the producers will be maximized if the weight loss and the fruit loss by damage are minimized. To compete in a saturated market and to attract consumers, the apples should have a fresh and undamaged appearance and a firm and crisp taste. In order to achieve these goals, the water transport processes should be carefully taken into consideration. On the one hand, producers try to reduce the weight loss as much as possible as evaporated water cannot be sold. Shriveling of the fruit, and thus a lack of fresh appearance and firm and crisp taste, is another disadvantageous effect of extended weight loss. On the other hand, Hatfield and Knee[1] indicated that controlled dehydration seems to be a promising application to reduce the bruising susceptibility of apples, as it reduces the turgor pressure in the surface cell layers. When the relationships between internal water profiles and quality parameters such as fresh appearance and susceptibility to bruise damage are known, it is possible to determine the optimum storage conditions. In this context, water transport processes in the fruit are to be modelled.

According to Luikov's basic laws of moisture transport,[2] the driving force under the isothermal conditions can be expressed in terms of gradients in water content. In this case, a homogeneous body and a linear relationship between water content and water potential are assumed. Fick's law for non-linear diffusion of water due to a difference in water content can then be used:

$$\frac{\partial \theta}{\partial t} = \nabla D(\theta) \nabla \theta \tag{1}$$

where D is the moisture diffusivity (m^2 s^{-1}), θ the moisture content (kg m^{-3}), t the time (s) and x the position (m).

When moisture transport takes place between different materials, the discontinuity of water content at the boundary of contact must be taken into consideration. The difference in water potential between the two materials is the driving force for moisture transport. Assuming a constant mass capacity within each material, this difference in water potentials can be expressed as a difference in water content.[2] In the case of apples in air, the equilibrium water concentration under the imposed conditions of air temperature and relative humidity is used instead of the true water content of the air to correct for the difference in properties of apples and air.

NMR imaging is a powerful tool for visualizing and monitoring water transport processes. Gummerson *et al.*[3] were the first to use NMR imaging techniques to monitor the dynamics of the internal water content distribution in several porous inorganic materials during capillary inflow. They estimated the diffusivity according to a technique outlined by Bruce and Klute[4] based on the application of the Boltzmann transformation to the non-linear diffusion equation. McCarthy *et al.*,[5] Schrader and Litchfield[6] and Pel *et al.*[7] used NMR

* *Correspondence to*: B. Nicolai, Flanders Centre for Postharvest Technology, K.U. Leuven, de Croylaan 42, B-3001 Heverlee, Belgium.
Contract/grant sponsor: IWT (Vlaams Institut voor de Bevordering van bet Wetenschappelijk-Technologisch Onderzoek in de Industrie.
Contract/grant sponsor: Flemish Minister for Science and Technology.
Contract/grant sponsor: FWO Vlaanderen (Flemish Fund for Scientific Research).

CCC 0749-1581/98/030196–09 $17.50

imaging to visualize internal water profiles in drying apple samples, a model food gel and porous building materials, respectively. With the numerical data from these images, an overall effective diffusion coefficient was calculated by McCarthy and Perez.[5] The estimation of the diffusivity was based on the best agreement between all experimental measurement points and simulated moisture profiles. The simulations were based on the equations of continuity for one-dimensional moisture transport, solved with the numerical finite difference method.[5]

In an extension to this, Schrader and Litchfield[6] assumed that the value of the moisture diffusivity would be affected by the local moisture content. Instead of using all the measurement points to calculate one value of the diffusivity, a value of the moisture diffusivity was calculated for each measurement point (in position and time). Simulations were performed with the finite difference method for the solution of the diffusion equation for radial diffusion in a cylinder. The optimization routine was based on the minimization of the squared error between measured and simulated moisture contents, for each measurement point. They concluded that, with the method used, the Fickian model did not accurately predict the internal moisture profiles.[6]

Pel *et al.*[7] numerically calculated moisture diffusivities as a function of moisture content. Their calculation was based on the integrated one-dimensional moisture diffusion equation. A very clear dependence of the value of the moisture diffusivity on the moisture content was observed. The behaviour of the moisture diffusivity was explained by the change in water transport mechanism with change in moisture content. At high moisture contents, the dominating mechanism is liquid moisture transport. With decreasing moisture content, the pores in the medium are drained and will therefore make a decreasing contribution to liquid transport, which leads to a lower moisture diffusivity. Below a certain critical moisture content, the dominating mechanism is moisture vapour transport, driven by differences in vapour pressure. With decreasing moisture content, the corresponding vapour pressure gradient increases, resulting in an increasing moisture diffusivity at very low moisture contents.[7] Favier and Chudek[8] also applied the NMR imaging technique to measure and model water diffusion in grains.

The objective of the work was to estimate both the apple flesh and skin diffusivity for water with the aid of NMR imaging in order to be able to predict the internal water content distribution in apples during storage under known conditions of air temperature and relative humidity.

EXPERIMENTAL

Fruit

Jonagold apples were collected from the experimental station at Rillaar (Belgium) in July 1995 [after 9 months of ultra-low oxygen (ULO) storage], February 1996 (after 4 months of ULO storage) and in May 1996 (after 7 months of ULO storage).

To determine the flesh diffusivity, cylindrical samples of 1.5 cm diameter and 2.5 cm length were cut radially from the apple fresh. The curved surfaces of the samples were covered with Vaseline. In this way, a one-dimensional drying geometry was realized which facilitated the estimation of the overal flesh diffusivity considerably. Fixed into a Plexiglas holder, only the flat surfaces of the flesh samples were exposed to drying. In the experiment to determine the skin diffusivity, the whole intact apple was exposed to drying.

NMR measurements and data analysis

The NMR equipment consisted of a Bruker 4.7 T Biospec spectrometer (^{1}H resonance frequency of 200 MHz) with a horizontal superconducting magnet (30 cm bore). In the experiments to determine the apple flesh diffusivity, the samples were positioned in cylindrical resonator coil (70 mm i.d.). A transmit/receive surface coil (15 mm diameter) was used in the experiments with the whole intact apple to zoom in on a small region near the skin and thus obtain a higher spatial resolution (about 39 μm) near the skin. The experimental set-up for both types of experiments is shown in Fig. 1.

In the first experiment (July 1995), apple flesh samples were allowed to dry for 10 h in an airstream at 30 °C and 30% relative humidity (RH). In Fig. 1 the experimental set-up is shown. During this drying period, coronal NMR images (slice thickness = 4 mm, FOV = 70 mm, matrix = 256 × 256, one acquisition, spatial resolution = 0.27 mm) were taken at regular time intervals using a spin-echo sequence (TR/TE = 6000/16 ms, imaging duration = 25 min). An example of such an image is given in Fig. 2, together with a detail of a flesh sample with water concentration profile. As a first approximation, the pixel intensity was assumed to be proportional to the water content during the whole experiment, as was also assumed by McCarthy and Perez.[5] To obtain water concentration profiles, the pixel intensities were scaled with a factor so that the average of the internal pixel values was equal to the average water concentration of the apple flesh, obtained from dried apple flesh samples. For each position (distance from the sample edge), the proton density was averaged over about 20 pixels perpendicular to the moisture flow direction to increase the signal-to-noise ratio. A few images with TE = 30 ms were taken, to detect variations in T_2 during drying.

In the second experiment (February 1996), apple flesh samples were allowed to dry for 7 h in an airstream at 22 °C and 62% RH. The RH was determined by means of a dew-point hygrometer. To correct for the effect of T_2 (change in the value of T_2 during drying or internal variation in the sample), one needs to extrapolate the echo signal amplitude to $TE = 0$. This was achieved using a multi-echo sequence (TR/TE = 6000/18–36–54–72 ms, slice thickness = 3 mm, FOV = 60 mm,

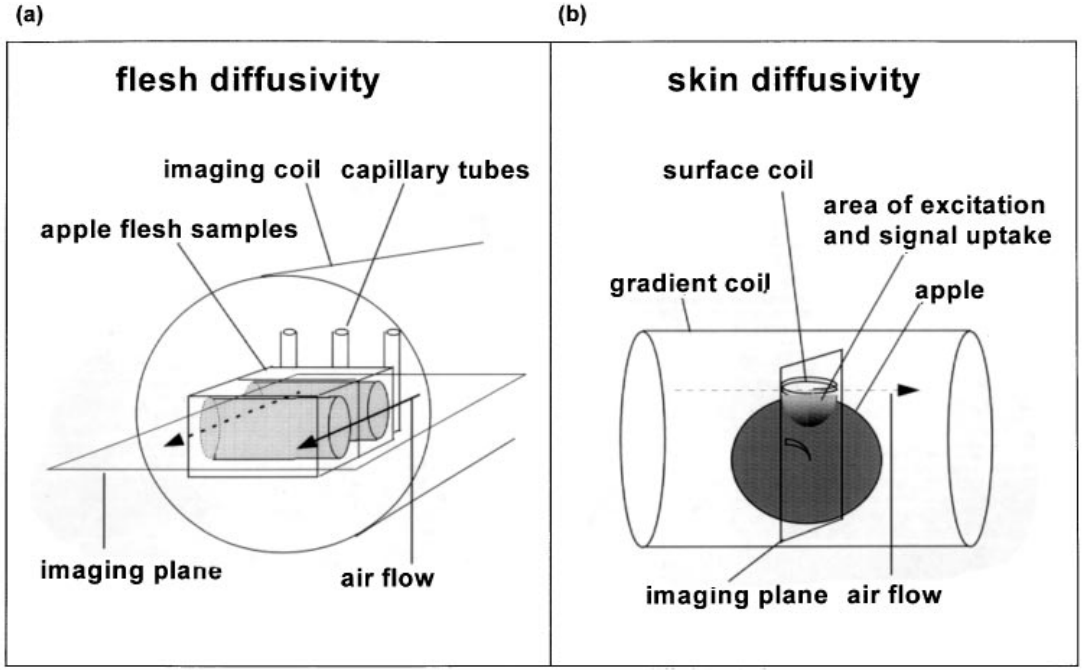

Figure 1. Experimental set-up for the measurements of (a) apple flesh and (b) skin diffusivity for water.

matrix = 256 × 256, one acquisition, spatial resolution = 0.23 mm, imaging duration = 13 min). The exact position of the edge of the samples was determined with an edge detection algorithm.

The damping of the required echo signals as a function of echo time TE was approximated by

$$I_{TE} = I_0 \exp(-TE/T_{2,\,\mathrm{app}}) \qquad (2)$$

with I_{TE} the intensity at echo time TE, I_0 the intensity at echo time $TE = 0$ or proton density, TE the echo time (ms) and $T_{2,\,\mathrm{app}}$ the apparent transverse relaxation time constant (ms) which includes spin–spin as well as spin–diffusion effects. The purpose of this approximation is solely to extrapolate, for each pixel, the echo intensity to $TE = 0$, which is taken as the water proton density value. A linear regression of the logarithm of the intensity value of each pixel *vs.* its corresponding echo time was calculated. The value for the proton density was derived from the intercept of this line. For each position (distance from the sample edge), the proton density was averaged over about 20 pixels perpendicular to the moisture flow direction to increase the signal-to-noise ratio. The proton density obtained was now supposed to be linearly related to the water concentration in the voxel. The effect of T_1 on the signal can be neglected because of the long TR. To obtain water concentration profiles, the pixel intensities were scaled with a factor so that the average of the internal pixel values

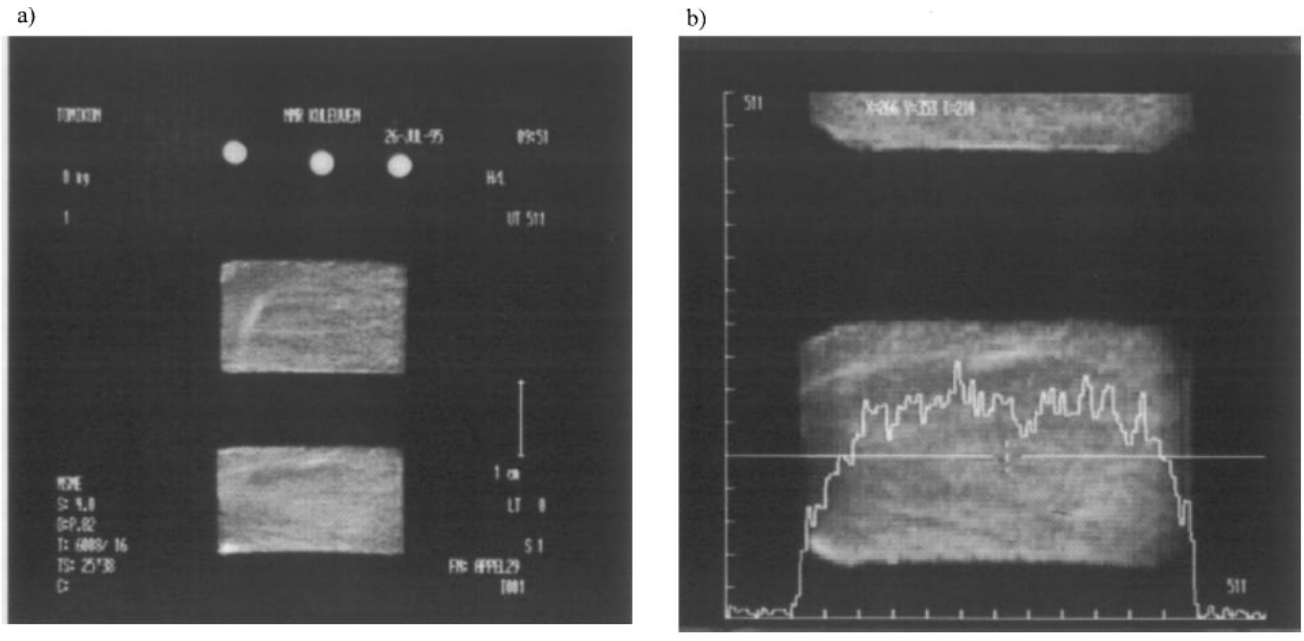

Figure 2. (a) Image of drying flesh samples and (b) detail with internal water profile.

was equal to the average water concentration of the apple flesh, obtained from dried apple flesh samples. In the third experiment (May 1996), apple flesh samples were allowed to dry for 12 h in an air stream at 23 °C and 25% RH. The imaging parameters and data manipulation were the same as in the second experiment.

In the fourth experiment (May 1996), a whole intact apple was allowed to dry for 7 days in an air stream at 20 °C and 0% RH (high-pressure air, dried at −60 °C). A multi-echo sequence was used (TR/TE = 6000/15–30–45–60 ms, slice thickness = 2 mm, FOV = 10 mm, matrix = 256 × 256, four acquisitions, spatial resolution = 0.039 mm, imaging duration = 103 min). An example of such an image is given in Fig. 3. The use of a surface coil has the advantage that the image FOV is reduced and that the spatial resolution is very high (39 μm in this case), but it has the disadvantage that the excitation (i.e. the value of the pulse angle) at a certain position in the sample, as well as the detected signal from this position, are determined by the distance of this position to the centre of the surface coil. The excitation power was adjusted so that the 90°/180° pulse condition was fulfilled in the immediate vicinity of the surface coil; the pulse angle and the signal intensity then roll off with increasing distance from the coil. To correct for this effect, a glass bulb (7 cm diameter) filled with water was placed in the same position as the apple and images were taken with the same parameters since we verified that the surface coil loading was unchanged. The decrease in intensity of the pixels in this image is due only to their distance from the coil centre. A parabola was fitted through these points. The intensity $I(x)$ of each pixel in the apple images was adjusted for the distance from the coil centre by the equation

$$I_{adj}(x) = I(x)[I^*(x)/I^*_0] \quad (3)$$

with $I_{adj}(x)$ the adjusted intensity at a distance x from the coil centre, $I(x)$ the intensity at a distance x from the coil centre, $I^*(x)$ the intensity in the water bulb at a distance x from the coil centre and I^*_0 the intensity in the water bulb at the coil centre. The exact position of the edge of the samples was determined with iterative selection of the threshold. An exponential fit of the intensity values at the different echo times yielded the proton density, T_2 and R^2 of the fit for each pixel. For each position (distance from the apple edge), an average proton density was calculated from about 30 lines around the axis of the coil. To obtain water concentration profiles, the pixel intensities were scaled with a factor so that the average of the internal pixel values was equal to the average water concentration of the apple flesh, obtained from dried apple flesh samples.

A gradient-echo (GE) image was made of the apple to visualize the thickness of the apple skin (FLASH sequence with TR/TE = 1000/6 ms). The GE image is very sensitive to susceptibility variations such as in the neighbourhood of flesh/air interfaces, resulting in signal void. As there are no air spaces in the skin, the signal does not decay as fast as in the apple flesh, and the skin appears as a bright line. An example of such a GE image is shown in Fig. 4. The bright line consisted of an average of three pixels, which corresponds to a skin thickness of about 120 μm.

Parameter estimation

In all simulations it was assumed that the diffusivity of apple flesh and skin does not depend on the moisture concentration as suggested by McCarthy *et al.*[5] As a consequence, Eqn (1) becomes linear, which simplified further analytical and numerical solutions. However, there are indications that this assumption is not valid for building materials[7] and model food gels[6] and further work is in progress to investigate the extent to

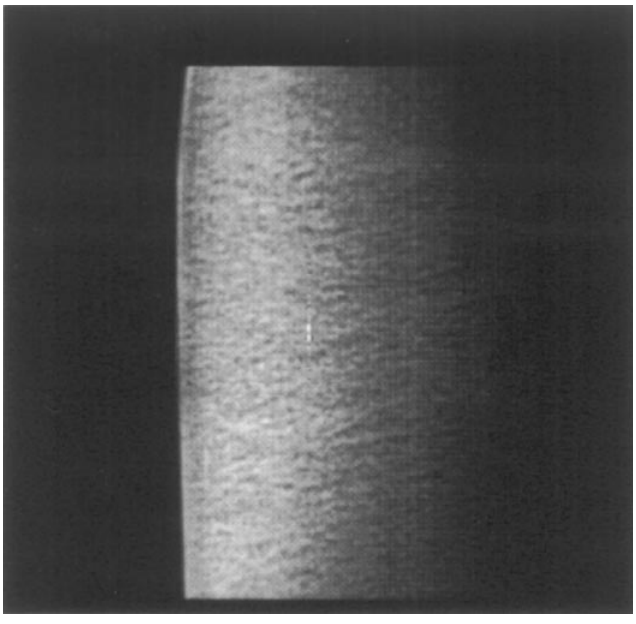

Figure 3. Image of whole drying apple.

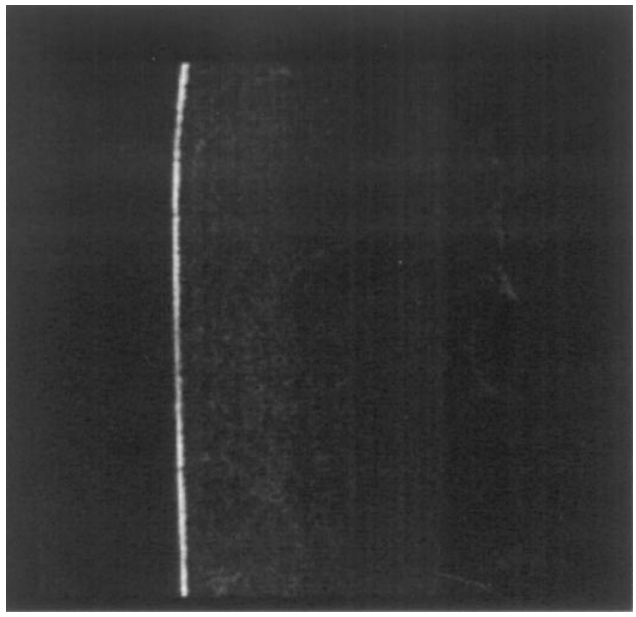

Figure 4. Gradient echo to visualize the skin taken with surface coil.

which the diffusivity of apple tissue and skin is independent of the moisture concentration.

The flesh diffusivity in the first, second and third experiments were estimated by minimization of the quadratic error between measured and simulated values. In the first experiment the analytical solution of Fick's law for one-dimensional diffusion was used to calculate the water concentration at positions spaced with the same resolution as in the imaging experiment and at times corresponding to the centre of the imaging periods. The initial water concentration distribution in the apple sample was assumed to be homogeneous. The corresponding value was obtained from drying apple samples at 70 °C until constant weight. The boundary condition was set as the equilibrium water concentration under the conditions of 30 °C and 30% RH. This value was obtained by keeping apple samples under these conditions until equilibrium (constant weight). The analytical solution of Fick's law under these conditions can be written as[9]

$$\theta(x, t) = \theta_e \operatorname{erfc}\left(\frac{x}{2\sqrt{Dt}}\right) + \theta_0 \operatorname{erf}\left(\frac{x}{2\sqrt{Dt}}\right) \qquad (4)$$

where θ_0 is the initial water concentration in the sample (kg m^{-3}) and θ_e the equilibrium water concentration of apple flesh under the conditions of the experiment (kg m^{-3}).

In the second and third experiments, a numerical solution with finite elements was chosen to correct for the spatial resolution in the imaging experiment, the imaging duration and inhomogeneities in the initial water concentration distribution in the sample. Since there are no analytical solutions available for Fick's law under these conditions, the partial differential equation was solved in a numerical way by using the finite element method.[10] The model consisted of a row of two-dimensional quadrilateral elements that are interconnected in a finite number of nodes. In every element the unknown moisture concentration can be approximated by a low-order interpolating polynomial. The element equations are obtained by applying the Galerkin weighted residual method, and the resulting first-order differential system was solved numerically.[11] The elements had a length equal to half the sample length and the mesh density corresponded to the experimental spatial resolution. At the drying boundary, the water concentration was set equal to the equilibrium water concentration for the imposed conditions of temperature and relative humidity. At the other end, corresponding to the middle of the sample, a no-flux boundary condition was set because of the symmetry. The initial conditions for each node were set as the corresponding water concentrations obtained from the first image taken during the drying experiment. A starting value for the flesh diffusivity was given and the simulation was run for the period of the drying experiment (time step 60 s). As the image duration was 13 min, 14 successive simulated water concentration profiles were averaged to correct for the imaging duration. The resulting water concentration values of the nodes of each corresponding element were then averaged again, to correct for the spatial resolution of the pixels in the image.

In the fourth experiment, two approaches were followed. In the first the flesh diffusivity was assumed to be known from the previous experiments and the skin diffusivity was estimated by means of a least-squares algorithm. The same finite element programme was used but now the model was approximated by a flat plate, neglecting the very small curvature in the considered area of pixels. The model consisted of a row of elements, with a length equal to the radius of the apple. The three outer elements were assigned to the skin and the other elements were assigned to the flesh. At the drying boundary, the water concentration was fixed to a value of zero. At the other end, corresponding to the middle of the apple, a no-flux boundary condition was set because of the symmetry. The initial conditions for each node were set as the corresponding water concentrations obtained from the first image taken during the drying experiment. Starting values for the skin and flesh diffusivity were given and the simulation was run for the period of the drying experiment (time step 26 min). As the image duration was 103 min, five successive simulated water concentration profiles were averaged from the starting time (x min after the first image was taken) of the image on. Similarly to the previous experiments, the resulting water concentration values of the nodes of each corresponding element were then averaged again, to correct for the spatial resolution of the pixels in the image. In a second approach, both the flesh and skin diffusivity were estimated simultaneously.

For the estimation of the flesh diffusivity from drying apple flesh samples, confidence intervals for the estimated parameter were obtained from the repetitions. In the fourth experiment, no repetitions were available. The standard deviations for skin diffusivity, or skin and flesh diffusivity, were estimated from the variance of the residuals and from the Jacobian matrix. The correlation between the two estimated parameters was also calculated according to.[12]

Gummerson *et al.*[3] used a technique suggested by Bruce and Klute[4] to estimate the moisture diffusivity of porous inorganic media. This technique is based on the application of the Boltzmann transform to the non-linear diffusion equation. As it involves the (ill-conditioned) calculation of derivatives of the transformed coordinate with respect to the moisture concentration, it is unsuitable for the present purpose, given the rugged appearance of the moisture concentration profile (see Fig. 2).

RESULTS

The estimated values of the flesh diffusivity for the first experiment are given in Table 1. The average value was 8.4×10^{-11} m^2 s^{-1}, with a relative standard deviation

Table 1. Estimated apple flesh diffusivities D_{flesh}, for water ($m^2\ s^{-1}$)

Replicate	Experiment 1	Experiment 2	Experiment 3
Rep. 1	5.46×10^{-11}	11.5×10^{-11}	7.64×10^{-11}
Rep. 2	4.31×10^{-11}	7.56×10^{-11}	11.6×10^{-11}
Rep. 3	14.5×10^{-11}	10.1×10^{-11}	9.25×10^{-11}
Rep. 4	9.23×10^{-11}	12.2×10^{-11}	12.2×10^{-11}
Average	8.4×10^{-11}	10.4×10^{-11}	10.2×10^{-11}
σ (RSD)	2.29×10^{-11} (27%)	2.07×10^{-11} (20%)	2.13×10^{-11} (21%)

(RSD) of 27%. In Fig. 5, some water concentration profiles obtained from the analytical solution and the estimated diffusivity values are shown together with the experimental water concentration profiles during the drying of the samples.

In Fig. 6, the intensity profiles for different echo times (16 and 30 ms) are shown, in addition to the ratio of the intensity at 16 ms ($I_{16\ ms}$) to that at 30 ms ($I_{30\ ms}$), for each pixel in a cross-section through the drying flesh samples. If the assumption of a constant T_2 was correct, the ratio of the intensity at different echo times should be constant, which is not the case. At the drying edges of the sample the $I_{16\ ms}/I_{30\ ms}$ ratio is higher than that in the sample centre. At the edges of the drying sample, less free water is present because of the evaporation. As free water has a higher T_2 than bounded water, areas with a lower content of free water, and thus a faster decay of the signal, will exhibit a higher $I_{16\ ms}/I_{30\ ms}$ ratio than areas with more free water such as the centre of the flesh samples. From the results of this experiment, it was concluded that a correction for changes in T_2 during drying is required. To solve this problem, a multi-echo sequence was used in the subsequent experiments. As can be seen from Fig. 5, large inhomogeneities were present in the flesh samples. The homogeneous initial condition was therefore abandoned in the subsequent experiments. By using finite elements, it is possible to correct for this and also for the spatial and time resolution, inherent to the experiments.

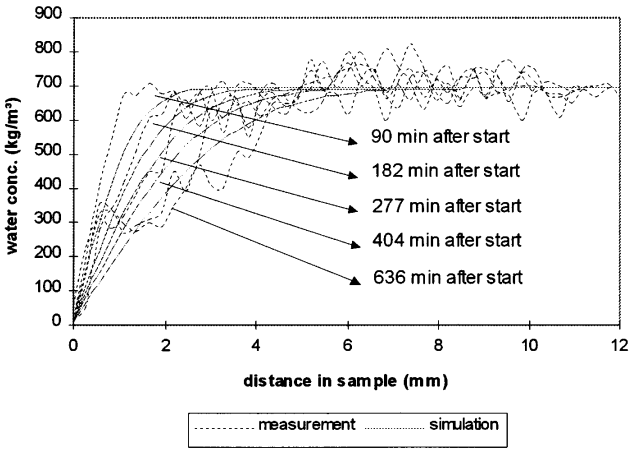

Figure 5. Simulated and experimentally measured water concentration profiles after different periods of drying for experiment 1.

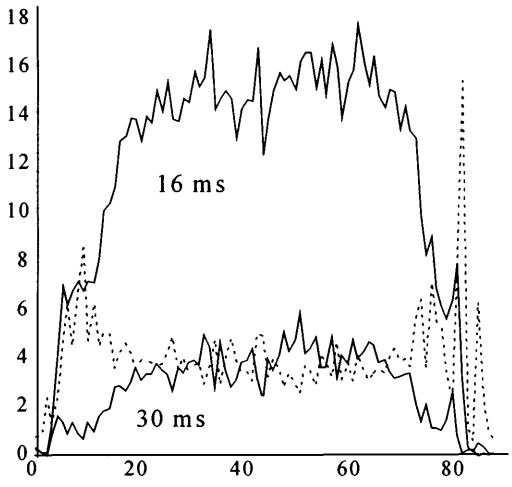

Figure 6. Internal intensity profiles (arbitrary units) through apple flesh sample after different echo times, and the ratio of these intensities for the first experiment. The dashed line is the ratio of the intensities at 16 and 30 ms.

In the second and third experiments, the flesh diffusivity values were 1.04×10^{-10} and $1.02 \times 10^{-10}\ m^2\ s^{-1}$, respectively (Table 1). In Figs 7 and 8, some corresponding simulated and experimental water concentration profiles for these experiments are shown. Figure 9 shows water concentration profiles during drying and the corresponding T_2 values, obtained from an exponential fit through four intensity values at different echo

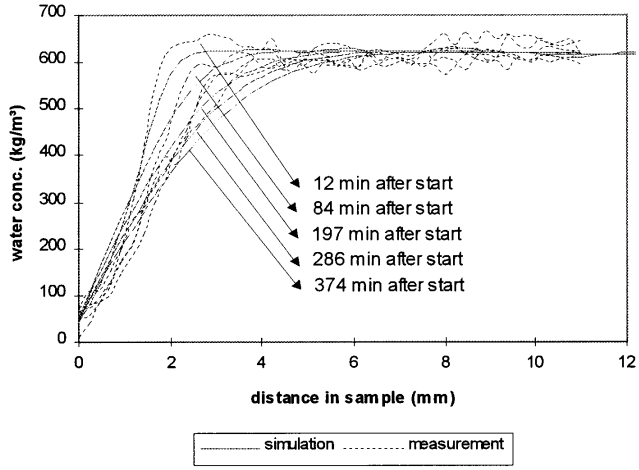

Figure 7. Simulated and experimentally measured water concentration profiles after different periods of drying for experiment 2.

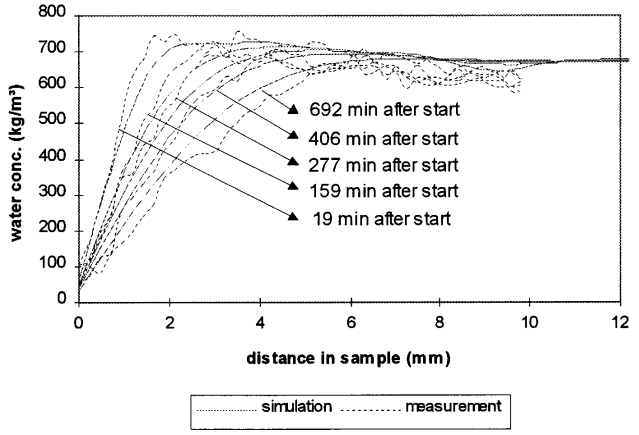

Figure 8. Internal water concentration profiles and T_2 profiles after different periods of drying in experiment 3.

times. In the initial measurement a higher T_2 is noticed at the recently cut edge. By cutting, cell walls and membranes were broken so that water was released. Before the evaporation started, the free water caused the T_2 near the edge to increase. It is clear that at the drying edges a lower T_2 was measured after some period of drying. This can be explained by the smaller amount of free water in these regions and it agrees with the findings of the first experiment. As can be seen from Table 1, the values of the flesh diffusivity for the different periods of ULO storage were not significantly different.

In the fourth experiment, it was assumed in a first approach that the value of the flesh diffusivity was known from the previous experiments. The average diffusivity value, 1.02×10^{-12} m^2 s^{-1}, was imposed for the pixels in the apple flesh. Minimization of the mean sum of squared errors then resulted in a value of 1.32×10^{-13} m^2 s^{-1} for the skin diffusivity, with an RSD of 5.4%. Experimental water concentration profiles and simulated profiles, obtained with these values for the skin and flesh diffusivity, are shown in Fig. 10(a). As the previous profiles do not seem to have a similar shape, simultaneous estimation of both parameters was performed in a second approach. The shape of the experimental water concentration profiles in this case was more similar to the simulated profiles, obtained with the estimated skin and flesh diffusivities, as is shown in Fig. 10(b). The flesh diffusivity value was 2.8×10^{-12} m^2 s^{-1} (RSD = 16%), which is about 30 times lower than the value from the experiment with the flesh samples. The corresponding skin diffusivity was 6.3×10^{-15} m^2 s^{-1} (RSD = 19%). The value of 0.43 obtained for the correlation coefficient between the skin and flesh diffusivity indicates that the parameters were not much correlated. The resulting RSDs were 16 and 19% for the flesh and skin diffusivity, respectively.

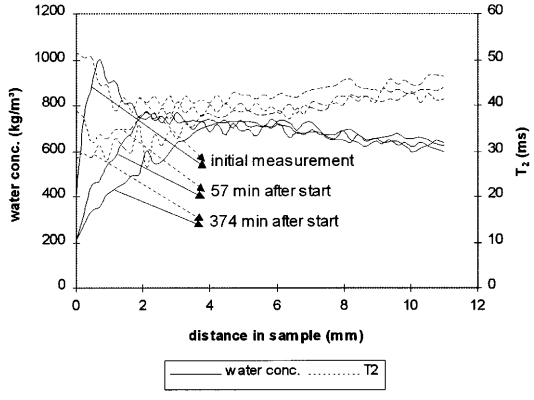

Figure 9. Internal water concentration profiles and T_2 profiles after different periods of drying in experiment 2.

CONCLUSIONS

Different drying experiments were carried out to obtain values for the skin and flesh diffusivity for water in apples. In the very dry parts of the samples, the T_2 was consistently lower, indicating a decrease in free water. From these results, it was concluded that a multi-echo sequence to correct for T_2 influences was required to obtain the water concentration. The estimated average flesh diffusivity was 10.3×10^{-11} m^2 s^{-1}. No significant differences were observed for apples after different periods of ULO storage. When the flesh and skin diffusivity were estimated simultaneously, the value of the flesh diffusivity was about 30 times lower than the value obtained from the experiments with the flesh samples. Similar results were obtained for the skin diffusivity. The correlation coefficient did not indicate a strong correlation between the parameters, and the RSDs of both estimated parameters were still reasonably low.

The observed discrepancies in the values for the moisture diffusivities can be attributed to several causes. First, during the drying of flesh samples the shrinkage was considerably more pronounced than during the drying of the intact apple. In the simulations, this shrinkage was not taken into account. Second, an important error source may be the edge detection, which can be experimentally distorted (an edge pixel may be partly empty). As the skin is only three pixels thick, an error of half a pixel may be considerable and will be investigated with a sensitivity analysis. A final explanation may be the dependence of the moisture diffusivity on the moisture content, described by other workers. This aspect is currently under investigation.

Acknowledgements

The authors thank the IWT (Vlaams Instituut voor de Bevordering van het Wetenschappelijk-Technologisch Onderzoek in de Industrie), the Flemish Minister for Science and Technology and the FWO Vlaanderen (Flemish Fund for Scientific Research) for providing financial support, which made this research possible. Bart Nicolaï is a Postdoctoral Research Fellow with the FWO Vlaanderen.

REFERENCES

1. S. G. S. Hatfield and M. Knee *Int. J. Food Sci. Technol.* **23**, 575 (1988).
2. A. V. Luikov, *Heat and Mass Transfer in Capillary Porous Bodies.* Pergamon Press, New York (1966).

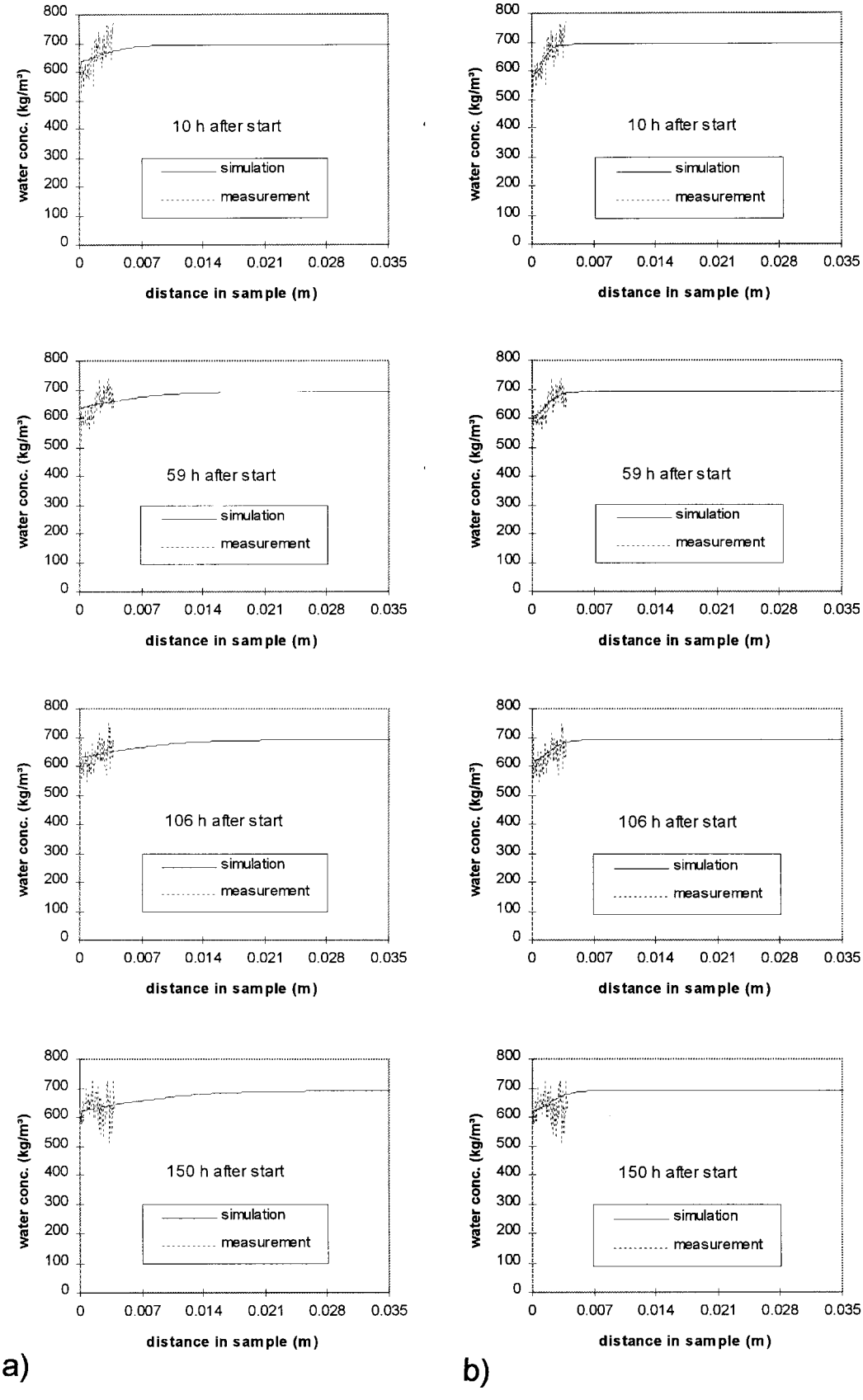

Figure 10. Simulated and experimentally measured water concentration profiles after different periods of drying. (a) Two-step estimation procedure; (b) simultaneous estimation of skin and flesh diffusivity.

3. R. J. Gummerson, C. Hall, W. D. Hoff, R. Hawkes, G. N. Holland and W. S. Moore, *Nature* (*London*) **281**, 56 (1979).
4. R. R. Bruce and A. Klute, *Soil Sci. Soc. Proc.* **20**, 458 (1956).
5. M. J. McCarthy, E. Perez and M. Ozilgen, *Biotechnol. Prog.* **7**, 540 (1991).
6. G. W. Schrader and J. B. Litchfield, *ASAE Paper* No. 91-6055 (1991).
7. L. Pel, H. Brocken and K. Kopinga, *Int. J. Heat Mass Transfer* **39**, 1273 (1996).
8. J. F. Favier and J. A. Chudek, paper presented at the XII CIGR World Congress on Agricultural Engineering, Milan, 1994.
9. C. J. Geankoplis, *Transport Processes and Unit Operations.* Prentice-Hall, Englewood Cliffs, NJ (1993).
10. Segerlind, *Applied Finite Element Analysis*, John Wiley & Sons, New York (1984).
11. N. Scheerlinck, B. M. Nicolaï, P. Verboven and J. De Baerdemaeker, ASAE Paper No. 96-3028 (1996).

